Ocean Systems Engineering, *Vol. 11, No. 1 (2021) 83-97*
DOI: https://doi.org/10.12989/ose.2021.11.1.083

Investigation of the U-shape submerged breakwater performance by the finite-different scheme

Mohammad Barzegar*

Department of Physical & Environmental Sciences, Texas A&M University-CC Corpus Christi, TX, USA

(Received August 12, 2020, Revised January 6, 2021, Accepted January 8, 2021)

Abstract. The submerged U-shape breakwater interaction with the solitary wave is simulated by the Boussinesq equations using the finite-difference scheme. The wave reflection, transmission, and dissipation (RTD) coefficients are used to investigate the U-shape breakwater's performance for different crest width, Lc1, and indent breakwater height, du. The results show that the submerged breakwater performance for a set of U-shape breakwater with the same cross-section area is related to the length of submerged breakwater crest, Lc1, and the distance between the crests, Lc2 (or the height of du). The breakwater has the maximum performance when the crest length is larger, and at the same time, the distance between them increases. Changing the Lc1 and du of the U-shape breakwaters result in a significant change in the RTD coefficients. Comparison of the U-shape breakwater, having the best performance, with the averaged RTD values shows that the transmission coefficients, K_t, has a better performance of up to 4% in comparison to other breakwaters. Also, the reflection coefficients K_R and the diffusion coefficients, K_d shows a better performance of about 30% and 55% on average, respectively. However, the model governing equations are non-dissipative. The non-energy conserving of the transmission and reflection coefficients due to wave and breakwater interaction results in dissipation type contribution. The U-shape breakwater with the best performance is compared with the rectangular breakwater with the same cross-section area to investigate the economic advantages of the U-shape breakwater. The transmission coefficients, K_t, of the U-shape breakwater shows a better performance of 5% higher than the rectangular one. The reflection coefficient, K_R, is 60% lower for U-shape in comparison to rectangular one; however, the diffusion coefficients, K_d, of U-shape breakwater is 35% higher than the rectangular breakwater. Therefore, we could say that the U-shape breakwater has a better performance than the rectangular one.

Keywords: Nwogu's extended Boussinesq equations; U-shape breakwater; rectangular submerged breakwater; RTD coefficients; finite difference method

1. Introduction

The coastal zone becomes a significant concern in many coastal cities due to their different uses as applying the coastal zone for building harbors and piers, mineral resources, fisheries, energy procurement, and recreational area. The presence of wave actions limits the use of coastal regions. The disturbance created by the incoming wave toward shorelines results in coastal erosion and accretion, and also it can have a devastating disaster for the harbor. Coastal erosion threatens the

*Corresponding author, Mr., E-mail: Mbarzegarpaiinlamouk@islander.tamucc.edu

http://www.techno-press.org/?journal=ose&subpage=7 ISSN: 2093-6702 (Print), 2093-677X (Online)

beachfront properties and causes the deduction of natural sources and valuable land across the shorelines that affect the tourism and shipping industries. The submerged breakwater is one of the widely applied methods to protect the coastline and harbor. The Submerged breakwaters have been constructed in the coastal zone to control the incoming wave with small and relatively high wave heights. However, submerged breakwaters create an issue for navigation. They are widely used due to economic reasons and tourism aspects, mainly where the visual limitation exists; also, they avoid the generation of the reflected wave, which affects the nearby shoreline.

One of the first offshore breakwaters was constructed at Winthrop Beach of the USA in 1935 (Chasten *et al*. 1993). The impact of the structure submergence, distance of structure to the shoreline, and crest width and shape of submerged breakwaters are not well understood. To better understanding of the impact of the mentioned parameters on shores, analytical investigation (Grue and Palm 1985, Matsui *et al*. 1991), laboratory and field experiments (Bogucki *et al*. 2020, Ghiasian *et al*. 2019 a, b, Esteban *et al*. 2017), and also numerical modeling (Ketabdari *et al*. 2014, 2015, Rahman *et al*. 2006, Rambabu *et al.* 2005) have been used. The analytical solutions for the wave-current interaction with a cylinder submerged breakwater have been derived by Matsui *et al*. (1991). Wang et al. (2019) conducted a numerical and experimental study to investigate the effects of the combination of the pneumatic breakwater and submerged breakwater on wave damping. Ghadimi *et al.* (2017) have used Nwogu's extended Boussinesq equation to simulate the wave propagation over the natural beach and composite submerged breakwaters. Zaghian *et al.* (2017) studied the interaction of solitary wave propagation over a submerged thin plate. Changing the plate angle towards the water surface causes wave height and wave speed reduction. Barzegar *et al.* (2020) have investigated the effects of the discontinuous-trapezoid submerged breakwaters on surf zone currents. Cannata *et al.* (2019) simulated the velocity field induced by discontinuous submerged breakwater over the beach ramp. Their three-dimensional model was compared with the experimental results, which show that the non-hydrostatic model can correctly simulate the fluid flow induced by wave-structures interaction.

The wave reflection, transmission, and dissipation (RTD) coefficients are the primary engineering concerns for wave propagation and interacting with a submerged breakwater. Morison (1949) investigated rectangular submerged breakwater's general effectiveness on both a horizontal and sloping bathymetry. Goda *et al.* (1967) found that the submergence ratio mostly governs the transmission coefficient in their laboratory experiment on vertical and composite overtopping breakwaters. Seeling (1980) observed that the breakwater submergence ratio is the most critical parameter to control the transmission coefficient. A mathematical model has been developed to compute the wave transformation over a porous structure (Rojanakamthorn *et al*. 1990). Garcia *et al.* (2004) simulated a numerical model to calculate the surface elevation in the presence of submerged breakwater. Dick and Brebner (1968) observed that the submerged breakwater with near-zero submergence could absorb 50% percent of the incoming wave energy. Raman *et al.* (1997) found that the submerged breakwater's crest width has an essential role in controlling the transmission coefficient. Dong *et al.* (2008) have experimentally investigated the wave transmission coefficients of three different floating breakwaters. They have conducted detailed experiments to investigate how the current velocity and other factors affect the wave transmission coefficients (Dong *et al.* 2008). Recently, the RTD coefficients are used by Tiao *et al*. (2019) to study the behavior of a pneumatic breakwater numerically. They found that wave parameters and airflow rate significantly influence the pneumatic breakwater's wave dissipation capacity. Barzegar *et al.* (2020) compared the performance of semicircular and rectangular submerged structures numerically. They observed that the transmission coefficient for rectangular breakwater for the same cross-section area

shows better performance than the semicircular one.

The lack of systematic study on the different shapes of the submerged breakwater and the breakwater design's economic aspect motivated us to investigate U-shape breakwater performance that has not been investigated. In this paper, the numerical simulation is used to study the performance of U-shape breakwater. The Nwogu's extended Boussinesq equations (Nwogu 1993) are considered to simulate the interaction of submerged breakwater and the solitary wave. The RTD coefficients are usually used to investigate the performance of the submerged breakwater. Finally, the U-shape breakwater results are compared with the rectangular breakwater to find which one has a better performance. The manuscript is organized as follows. The governing equation and the numerical model are presented in sections 2 and 3. The validation test is described in section 4. The results and comparison of breakwaters are discussed in section 5, and finally, the summary and conclusion are summarized in section 6.

2. Governing equations

The incompressible Navier-Stokes equation is the start point for modeling the interaction of surface water waves with structures. The numerical modeling of the Navier-Stoke equations is complicated for a three-dimensional flow. For this reason, it is common to simplify the equations with some assumptions. The Navier-Stokes equation is simplified to the Boussinesq equation by assuming an incompressible and irrotational flow. Peregrine (1972) provides a mathematical framework for the derivation of the water wave equation that its dispersion relation is only an accurate approximation to the stokes first-order wave theory. Madsen *et al*. (1996) have improved the dispersion relation of Peregrine for the Boussinesq equations. Later *et al*. (1996) enhanced the equations by creating a variable depth extended Boussinesq equation by changing the Peregrine's Boussinesq equations. Nwogu (1993) has made the equations more compatible with shallow water by using the velocity at an arbitrary depth as a dependent variable and derived the extended Boussinesq equations.

Numerical modeling of wave and submerged breakwater interaction requires the governing equations to simulate the wave movement from deep water to shallow water. Therefore, the one dimensional-extended Boussinesq equations derived by Nwogu (1993) for the conservation of mass and momentum is used

$$\frac{\partial \eta}{\partial t}+\frac{\partial}{\partial x}[(h+\eta)u]+\frac{\partial}{\partial x}\left[\left(\frac{\left(\frac{Z_\alpha}{h}\right)^2}{2}-\frac{1}{6}\right)h^3\left(\frac{\partial^2 u}{\partial x^2}\right)+(\frac{Z_\alpha}{h}+\frac{1}{2}\quad)h^2\left(\frac{\partial^2(hu)}{\partial x^2}\right)\right]=0 \tag{1}$$

$$\frac{\partial u}{\partial t}+g\frac{\partial \eta}{\partial x}+u\frac{\partial u}{\partial x}+\frac{(\frac{Z_\alpha}{h})^2}{2}h^2\frac{\partial}{\partial t}\left(\frac{\partial^2 u}{\partial x^2}\right)+Z_\alpha\frac{\partial}{\partial t}\left(\frac{\partial^2(hu)}{\partial x^2}\right)=0 \tag{2}$$

where η and h are the surface elevation and water depth, respectively. g is gravity acceleration, u is the horizontal velocity at an arbitrary depth of $Z_\alpha = 0.531\ h$. The mass and momentum conservation equations are rewritten to facilitate the later application of a numerical model with a higher-order time-stepping procedure.

$$\eta_t = \ E(\eta,u) \tag{3}$$

$$[U(u)]_t = \ F(\eta, u) \tag{4}$$

The E and F quantities on the right side of the Eqs. (3) and (4) are

$$E(\eta, u, v) = -[(h+\eta)u]_x - \{\ \alpha_1 h^3 (u_{xx}) + \alpha_2 h^2 [(hu)_{xx}\ \}_x \tag{5}$$

$$F(\eta, u) = -g\eta_x - \frac{1}{2}(u^2)_x \tag{6}$$

The time derivative is denoted by a subscript t, and the subscript x presents the derivative of the terms in the x-direction. The term of $[U(u)]_t$ is

$$[U(u)]_t = [\ u + h[\ b_1 h\ u_{xx} + b_2 (hu)_{xx}]]_t \tag{7}$$

where α_1, α_2, b_1, and b_2 are defined as

$$\alpha_1 = \ \frac{\theta^2}{2} - \frac{1}{6} \quad ; \quad \alpha_2 = \theta + \frac{1}{2} \quad ; \quad b_1 = \frac{\theta^2}{2} \quad ; \quad b_2 = \theta \tag{8}$$

Where θ is defined as $\theta = \frac{Z_\alpha}{h}$.

3. Numerical model

3.1. Mesh discretization

A staggered grid system for the spatial domain is used to discretize the various term in continuity and momentum equations (Fig. 1). The Velocity vector components are located on the interface of the cells, and the water surface elevations (η) and water depths (h) are placed at the cell center that they are referred to by subscript indices $i = 1,2,\dots,m$, increasing in the x-direction. The mesh is sized equally in the x-direction (Δx), and the time step is shown by (Δt). The scalar term, located at the cell interfaces, is obtained by the linear interpolation

$$(h+\eta)_{i+1/2} = \frac{1}{2}(h_i + h_{i+1}) + \frac{1}{2}(\eta_i + \eta_{i+1}) \tag{9}$$

3.2. Discretization of the governing equations

The time integration is applied to the governing equations by the fourth-order accurate Adams predictor-corrector method (Wei and Kirby 1995).

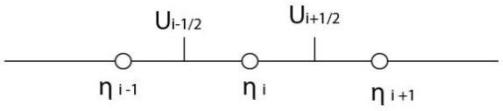

Fig. 1 The grid system used in the model

In the predictor step, the explicit third-order Adams-Bashforth method is implemented to the governing Eqs. (5) and (6).

$$\eta_{i,j}^{n+1*} = \eta_{i,j}^{n} + \frac{\Delta t}{12}[23E_{i,j}^{n} - 16E_{i,j}^{n-1} + 5E_{i,j}^{n-2}] \tag{10}$$

$$U_{i+1/2,j}^{n+1*} = U_{i+1/2,j}^{n} + \frac{\Delta t}{12}\left[23F_{i+\frac{1}{2},j}^{n} - 16F_{i+\frac{1}{2},j}^{n-1} + 5F_{i+\frac{1}{2},j}^{n-2}\right] \tag{11}$$

The superscript n, in Eqs. (10) and (11), refers to the present time; therefore, all terms on the right-hand side of the Eqs. (10) and (11) are known from the previous calculation. The value of $\eta_{i,j}^{n+1*}$ is directly obtained by Eq. 10 and the $U_{i+1/2,j}^{n+1*}$ has calculated by using the simultaneous solution of the matrix equation. The terms of $\mathrm{F}_{\mathrm{i}+\frac{1}{2},\mathrm{j}}^{\mathrm{n}+1*}$ and $F_{i+\frac{1}{2},j}^{n+1*}$ are used in Eqs. (5) and (6) to calculate the corresponding values of $E_{i,j}^{n+1*}$ and $F_{i+\frac{1}{2},j}^{n+1*}$. These values are utilized in the corrector step with the fourth-order Adams-Moulton method to calculate the correct values of $\eta_{i,j}^{n+1}$ and $U_{i+\frac{1}{2},j}^{n+1}$.

$$\eta_{i,j}^{n+1} = \eta_{i,j}^{n} + \frac{\Delta t}{24}[9E_{i,j}^{n+1*} + 19E_{i,j}^{n} - 5E_{i,j}^{n-1} + E_{i,j}^{n-2}] \tag{12}$$

$$U_{i+\frac{1}{2},j}^{n+1} = U_{i+\frac{1}{2},j}^{n} + \frac{\Delta t}{24}\left[9F_{i+\frac{1}{2},j}^{n+1*} + 19F_{i+\frac{1}{2},j}^{n} - 5F_{i+\frac{1}{2},j}^{n-1} + F_{i+\frac{1}{2},j}^{n-2}\right] \tag{13}$$

The predictor-corrector method will be iterated until the numerical error between two sequential results for the corrector section reaches a required limit. The numerical error is calculated by $\Delta f = (\sum_{i,j} | f_{i,j}^{n+1} - f_{i,j}^{(n+1)^p} |) / (\sum_{i,j} | f_{i,j}^{n+1} |)$, where f can be η and u. In this paper, the predictor-corrector iteration is stopped when $\Delta \mathrm{f} < 0.001$. Spatial discretization is required for the first and second-order spatial derivatives. For instance, the fourth-order accurate four-point central difference scheme is used to calculate the first-order derivative of u

$$\{\frac{\partial u}{\partial x}\}_i = \frac{u_{i-\frac{3}{2}} - 27u_{i-\frac{1}{2}} + 27u_{i+\frac{1}{2}} - u_{i+\frac{3}{2}}}{24\Delta x} \tag{14}$$

For the first-order derivative of $\partial \mathrm{u}^2 / \partial \mathrm{x}$, the four-point central difference scheme is

$$\{\frac{\partial u^2}{\partial x}\}_{i+1/2} = \frac{u^2{}_{i-\frac{3}{2}} - 8u^2{}_{i-\frac{1}{2}} + 8u^2{}_{i+\frac{3}{2}} - u^2{}_{i+\frac{5}{2}}}{24\Delta x} \tag{15}$$

A Von Neuman stability analysis is used by Lin and Man (2007) to analyze the stability of the Nwogu's Boussinesq equations. They found that the predictor and corrector steps are stable when the $Cr = \sqrt{gh}(\frac{\Delta t}{\Delta x})$ is less than or equal one for the predictor step and 0.5 for the corrector step. In this work, the same criteria are used for the stability condition.

3.3 Boundary conditions

Proper boundary conditions are essential to run the numerical model properly. In this paper, two boundary layers are used, absorbing the boundary layer and the internal generation of waves.

3.3.1Absorbing boundary

An absorbing boundary is used to absorb the energy of the wave, and the perfect one should not be allowed a wave reflection to occur. The absorbing layer with a *Ls* length is applied at the end of the numerical tank in this paper. The damping terms are added to the momentum equation

$$[U(u)]_t = F(\eta, u) - w1(x)u - w2(x)u_{xx} \tag{16}$$

Where the second-order derivative is analogous to the linear viscous terms in the Navier-Stokes equations (Israeli and Orszag 1981). The damping coefficients are defined as

$$w1(x) = \begin{cases} 0; & x < x_s \\ \alpha_1 \omega f(x); & x > x_s \end{cases} \tag{17}$$

$$w2(x) = \begin{cases} 0; & x < x_s \\ \alpha_2 \upsilon f(x); & x > x_s \end{cases} \tag{18}$$

Where α_1 and α_2 are constants to be determined for the specific running. ω is the frequency of the wave to be damped, and υ is the viscous coefficient. x_s is starting coordinate of absorbing layer and $f(x)$ is presented as

$$f(x) = \frac{exp(\frac{x-x_d}{L_s})^n - 1}{exp(1) - 1} \tag{19}$$

Where the *Ls* is the absorbing layer width that it is usually taken to be between two to three times of wavelength.

3.3.2 Internal generation of solitary wave

The solitary wave solution for Nwogu's model equations is used (Wei and Kirby 1995). The surface elevation, η, and horizontal velocity, u, of solitary wave are expressed as

$$\eta(x,t) = A_1.sech^2[B(x - ct)] + A_2.sech^4[B(x - ct)] \tag{20}$$

$$u = A.sech^2[B(x - ct)] \tag{21}$$

Where c is wave velocity, $c = \sqrt{g(H + h)}$, and H is the solitary wave height. A, A_1, A_2, and B are defined as

$$A = \frac{c^2 - gh}{c} \tag{22}$$

$$B = \{\frac{c^2 - gh}{4[\left(\alpha + \frac{1}{3}\right)gh^3 - \alpha h^2 c^2]}\}^{1/2} \tag{23}$$

$$A_1 = \frac{c^2 - gh}{3[\left(\alpha + \frac{1}{3}\right)gh - \alpha c^2]} h \tag{24}$$

$$A_2 = -\frac{(c^2 - gh)^2}{2ghc^2} \frac{[\left(\alpha + \frac{1}{3}\right)gh + 2\alpha c^2]}{[\left(\alpha + \frac{1}{3}\right)gh - \alpha c^2]} h \tag{25}$$

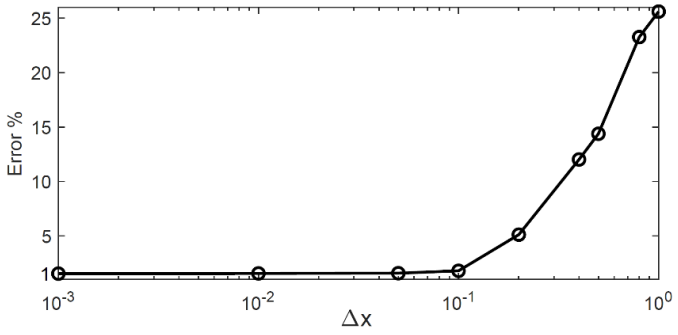

Fig. 2 Mesh convergence test. The ratio of $\frac{\Delta x}{\Delta t} = 10$ was constant for different Δx. The height of the solitary wave is $H = 0.05$ m, and water depth equals h= 0.5 m. The error, $100*(H - H_{numerical})/H$ was measured after the wave propagates for t= 50 s, where $H_{numerical}$ is calculated by the numerical model

Where α is defined as $\alpha = \frac{1}{2}{Z_\alpha}^2 + Z_\alpha$.

4. Validation tests

The numerical scheme is tested to assess the ability of the model on the simulation of the solitary wave interaction with U-shape breakwater. The first test is the propagation of solitary over the flat bottom for a long time, and the second test is the interaction of the solitary wave with a simple breakwater shape.

4.1 The propagation of solitary wave

The solitary wave equations of 20 and 21 are used as an initial condition for the solitary wave to test the numerical model for a long simulation time. The test is a standard test to analyze the conservative and stability properties of the numerical scheme (Wei and Kirby 1995). The solitary wave with a height of H=0.05 m propagates over a flat bottom for t=50 s and 100 s. The length of the channel is L=300 m. The water depth is h=0.5 m, and the initial position of the solitary wave is x=20 m. The mesh convergence test was conducted to indicate the appropriate mesh size (Fig. 2). Fig. 2 shows that for constant $\frac{\Delta x}{\Delta t} = 10$, the measured-wave height error becomes approximately constant for $\Delta x < 0.1$. The numerical modeling gets very expensive in the point of view of computational time for $\Delta x < 0.01$; therefore, the grid size is considered $\Delta x = 0.01$. To satisfying the $Cr = \sqrt{gh}(\frac{\Delta t}{\Delta x})$ criteria which has to be less than or equal one, the time step is considered to be $\Delta t = 0.001$ s. Our numerical results are compared to the analytical solution (Eqs. (20) and (21)). The comparison of numerical results at time t=50 s and 100 s (Fig. 3) shows that the wave height remains constant for a long distance, and there is a small phase change relative to the analytical solution for both times. The small deduction of wave height presents the rather good conservative and stability properties of the numerical model to run for a long distance.

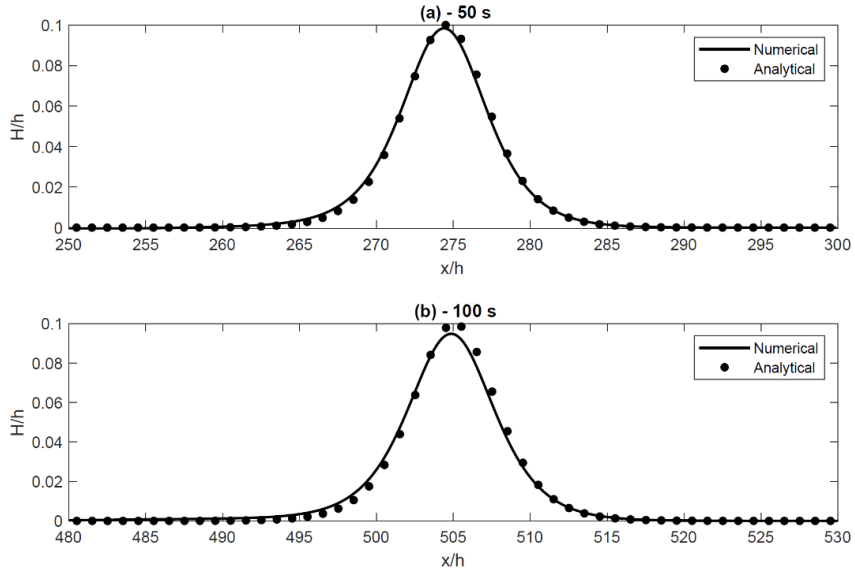

Fig. 3 Comparison of the numerical model and analytical solution of the solitary wave for propagating time of t= 50 s (a) and t =100 s (b)

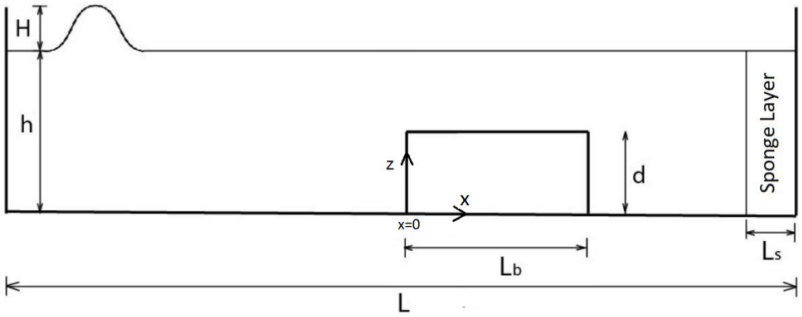

Fig. 4 Numerical setup of solitary wave transformation over a rectangular submerged breakwater. The wave is generated at the left part of the channel and passes over the breakwater. Two gauges are located at the left ($x = -8.2$ m) and the right side ($x = 0.44$ m) of the coordinate center, x=0

4.2 Interaction of solitary wave with a rectangular submerged breakwater

The submerged breakwater is used to reduce the incoming wave height. The rectangular breakwater has one of the simplest shapes, and it is easy to be settled in the water. The test is considered to analyze the nonlinear effects of the numerical scheme. The left edge of the breakwater with a height of d=0.08 m and length of L_b=0.4 m is located at x=0 (Fig. 4). The solitary wave is propagated from left to right with the initial position of x= 20 m. The wave height is $H = 0.0288$ m, and the channel length is L = 200 m. The sponge layer is located at x_s =195 m with a length of Ls=5 m. The water height is h=0.16 m, and the grid size and time step are $\Delta x = 0.01$ m

and $\Delta t = 0.001$ s, respectively. Two gauges are considered at x = -8.2 m and x = 0.44 m to measure the wave height. The computed results for the wave height is shown in Fig. 5. The small difference between the numerical model and experimental results reveals that the model can simulate wave and submerged breakwater interaction.

5. Performance of the U-shape submerged breakwater

The U-shape submerged breakwater performance for different crest lengths ($Lc1$) and indent breakwater height (du) are compared via the RTD coefficients. In the following, the determination of the RTD coefficients and the numerical model implementation are presented.

5.1 Determining the RTD coefficients

Colliding the wave with breakwater results in the absorption of a part of wave energy. The rest of the energy is reflected and passed through the breakwater. The RTD coefficient usually investigates the performance of a submerged breakwater. A better choice of geometry could be determined for the submerged breakwater by comparing the RTD coefficients values, i.e., the coefficients of reflection (K_r), transmission (K_t) and dissipation (K_d).

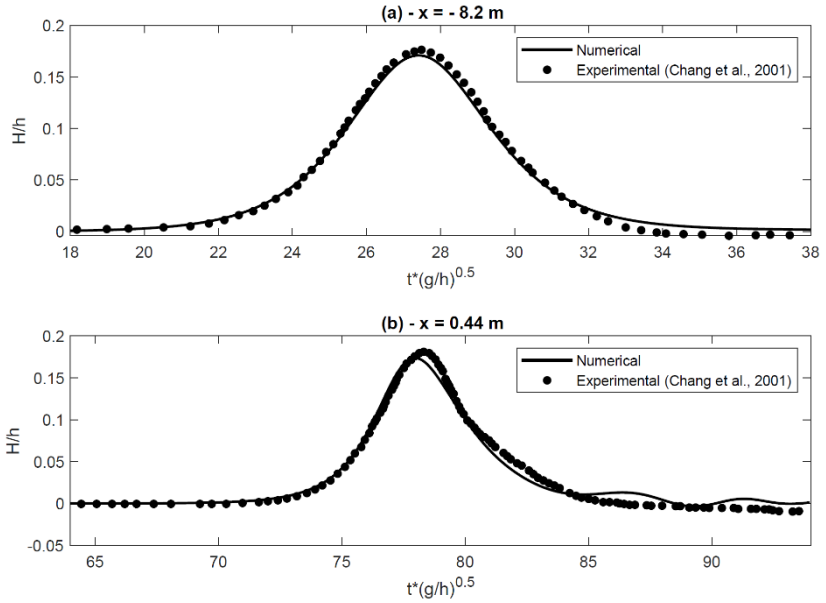

Fig. 5 Time history of the numerical and experimental solitary wave surface elevations at $x = -8.2$ m (a) and $x = 0.44$ m (b). The height of the solitary wave is $H = 0.0288$ m, and water depth equals h= 0.16 m

The reflection coefficient, $K_r = (\frac{H_r}{H})$, is the ratio of the reflected wave height (H_r) to the incident wave height (H) and the transmission coefficient, $K_t = (\frac{H_t}{H})$, is the ratio of the transmitted wave height (H_t) over the breakwater to incident wave height (Lin 2004, Lin and Karunarathna 2007). The numerical results indicate that the wave interactions with breakwater structures generate non-energy conserved K_R and K_T. This, in turn, yields a dissipative type of contribution K_D (Dissipation coefficient) which is defined as $K_d = \sqrt{1-(K_r)^2-(K_t)^2}$.

5.2 Model implementation

The building cost of the submerged breakwater is a significant factor in designing the shape of the breakwater. In this paper, we want to see how the U-shape submerged breakwater improves the economic cost. For this purpose, the U-shape submerged breakwater is considered on the numerical channel with a length of *L*=300 and a water depth of *h*= 1 m (Fig. 6). The solitary wave, with a height of *H*= 0.5 m, is propagated from the initial position of *x*=20 m located at the left side of the channel. The sponge layer was placed on the right side of the channel with a length of *Ls*=5 m to absorb the incoming wave. The U-shape submerged breakwater center is located at *x* =270 m for all runs mentioned in Table 1.

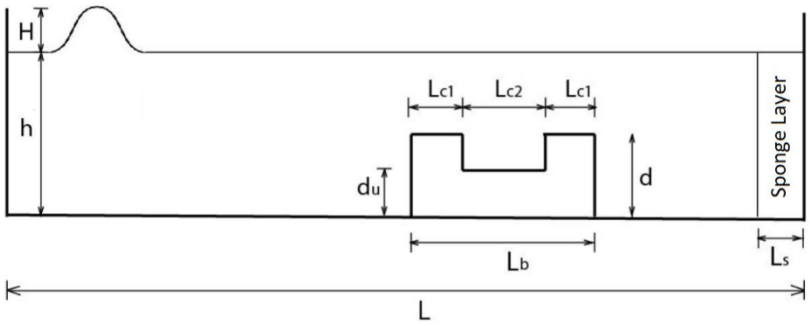

Fig. 6 A scheme of the numerical channel and a U-shape submerged breakwater

Table 1 Dimensions of the U-shape submerged breakwaters. The table presents the length of *Lc2* for different *Lc1* and *du*. The dimensions are in the meter unit. The cross-section area of all breakwaters are constant, and it equals 0.5 m^2

$d_{u\,(m)}$ \ *Lc1(m)*	0.4	0.3	0.2	0.1
0.4	0.25	0.5	0.75	1
0.3	0.33	0.66	1	1.33
0.2	0.5	1	1.5	2
0.1	1	2	3	4

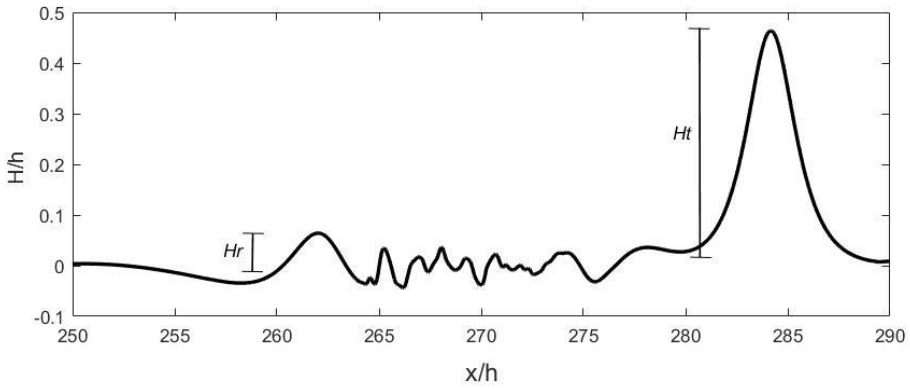

Fig. 7 The solitary wave height after passing the U-shape submerged breakwater. The breakwater center is located at $x/h = 270$. The incoming wave height is $H/h = 0.5$

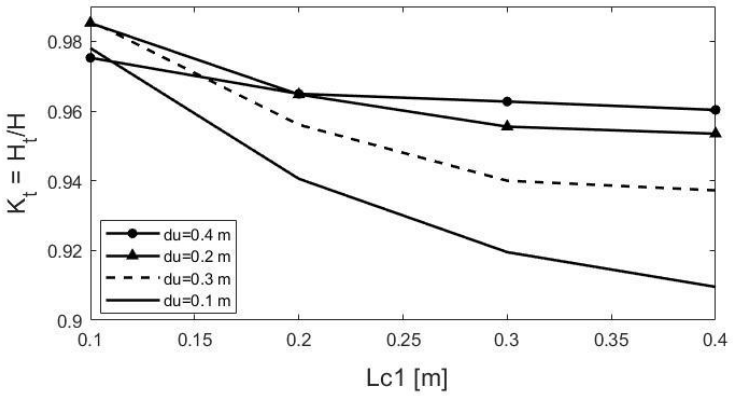

Fig. 8 Distribution of K_t coefficients for the U-shape submerged breakwater. The wave height and water depths are $H = 0.5\ m$ and $h = 1$ m, respectively

We compare the U-shape breakwaters for different *Lc1* and *du*. *Lc1* is the width of the breakwater crest, and *du* is indent breakwater height. In all breakwaters, the cross-section area is constant, 0.5 m^2. The breakwater height is constant, *d*=0.5 m for all runs, and the L_b changes based on the value of *Lc1* and *du*. The related dimension of each breakwater is given in Table 1. The grid size and time steps are $\Delta x = 0.001$ m and $\Delta t = 0.0001$ s, respectively. The grid size and time step are considered small enough to simulate better the effects of the implemented changes on the breakwater. The computed wave height for the submerged breakwater with *Lc1*= 0.4 m and *du*= 0.4 m is shown in Fig. 7. The transmission wave height, H_t is measured when the wave crest passes the breakwater at a distance of 2 m. The maximum amplitude of the tail is determined as the reflected wave height, H_r.

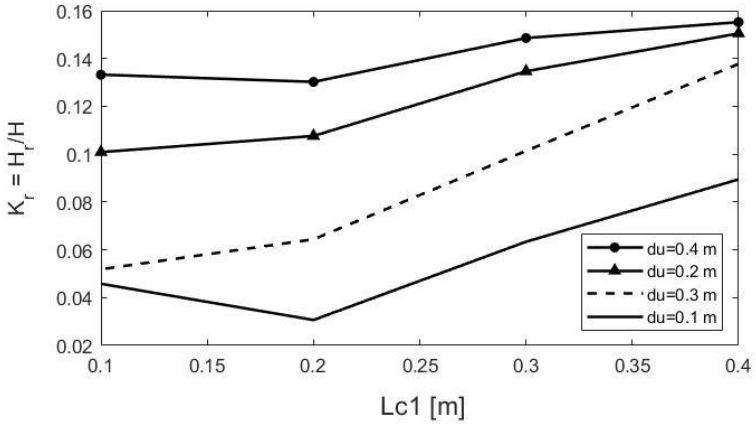

Fig. 9 Distribution of K_r coefficients for the U-shape submerged breakwater. The wave height and water depths are $H = 0.5\ m$ and $h = 1$ m, respectively

5.3 RTD Coefficients

The RTD coefficients are presented in Figs. 8-10 to compare the performance of breakwaters for different *Lc1* and *du*. In this paper, when it is expressed that *Lc1* is constant and the value of *du* increases, it means that the distance between the crest of breakwater increases. In other words, the value of *Lc2* increases. Also, *du* is constant, and *Lc1* is increased, which means that the distance between the breakwater crest, *Lc2*, decreases. For a constant *du*, the K_t decreases when *Lc1* increases (Fig. 8). It shows the performance of the submerged breakwater is related to the width of the breakwater crest. On the other hand, the comparison of the K_t coefficients for constant *Lc1* shows that the K_t decreases for smaller du values, i.e., the distance between the crest of U-shape breakwater, *Lc2*, plays a significant role in the transmitted wave height. It has resulted that the performance of the submerged breakwater is related to the length of the submerged breakwater crest, *Lc1*, and the distance between the crests, *Lc2*. The breakwater with dimensions of *Lc1* = 0.4 m, *du* = 0.1 m, and *Lc2* = 1 m has the best performance among all breakwaters in this paper, and its performance is as follows. The K_t coefficient shows better performance up to 4% in comparison to other breakwaters (Fig. 8). Also, the K_r coefficients have a better performance of 55% on average in comparison to other breakwaters. The K_t coefficients represent the manner as the K_r coefficients (Fig. 9). The K_d coefficients have a better performance of about 30% on average (Fig. 10). However, the model governing equations are non-dissipative.

The model equation is derived from the potential theory and has no dissipation mechanism. The momentum equation in (2) does not have either bed friction or turbulent diffusion terms. The energy should be, therefore, be conserved in the system, and thus incident wave energy should be balanced with reflected and transmitted wave energy. Wave energy cannot be measured by wave height only, as in the case of linear periodic wave propagation. Both reflected and transmitted waves are no longer solitary waves, and their crest height does not represent their total energy. Therefore, the resulting reflection-transmission energy inconsistency is called energy dissipation here. In other words, the non-energy conserving of the transmission and reflection coefficients due to the interaction of wave and breakwater results in dissipation type contribution.

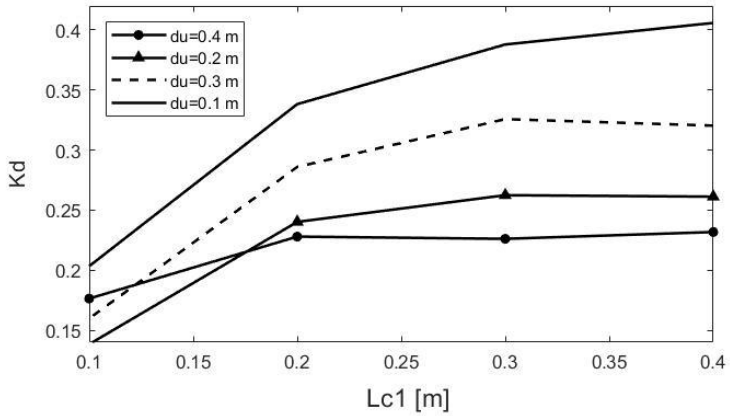

Fig. 10 Distribution of K_d coefficients for the U-shape submerged breakwater. The wave height and water depths are $H = 0.5\ m$ and $h = 1$ m, respectively

The implementation and designing of a breakwater are amalgamated with the cost analysis. For this reason, the U-shape breakwater with the best performance is compared with the rectangular breakwater with the same cross-section area of 0.5 m^2. The dimensions of the rectangular breakwater are Lb = 1 m and d = 0.5 m. The RTD coefficients of the rectangular breakwater are $K_t = 0.95$, $K_r = 0.15$, and $K_t = 0.26$. The U-shape breakwater has a better performance of 5% for K_t, and 60% for K_r. The K_d coefficient of U-shape breakwater is 35% higher than the rectangular breakwater.

6. Conclusions

In this paper, the Boussinesq equations have been used to simulate submerged U-shape breakwater interaction with the solitary wave. The RTD coefficients are used to investigate the U-shape breakwater's performance for different crest width, *Lc1*, and the indent breakwater height *du*.

The results represent that the submerged breakwater performance is related to the length of the submerged breakwater crest, *Lc1*, and the distance between the crests, *Lc2*. In other words, the breakwater has the maximum performance when the length of the crest is larger, and at the same time, the distance between them increases. The U-shape breakwater with dimensions of *Lc1*=0.4 m, *du*=0.1 m, and *Lc2*=1 m has the best performance among all breakwaters in this paper. The K_t and K_d coefficients have better performance by up to 4% and 30% in comparison to other breakwaters. The K_r coefficients show that the submerged breakwater with smaller K_t has a smaller K_r coefficients. The K_r coefficients have a better performance of 55% on average in comparison to other breakwaters.

Finally, to investigate the U-shape breakwater's economic advantages, the breakwater is compared with rectangular breakwater with the same cross-section area. The RTD coefficients of the rectangular breakwater are $K_t = 0.95$, $K_r = 0.15$, and $K_t = 0.26$. The U-shape breakwater has a better performance of 5% for K_t, and 60% for K_r. The K_d coefficient of U-shape breakwater is 35% higher than the rectangular breakwater.

As the U-shape breakwater performance is related to the distance between the crests, future work could be undertaken to study the relation of the distance and wave height and amplitude.

Acknowledgments

I would like to thank Hasan Jafari and Behnam Barzegar for their technical help.

References

Barzegar, M., Ketabdari, M. J., Kayhan, K. and Palaniappan, D. (2020), "Boussinesq Modelling of Waves and Currents in the Presence of Submerged Detached/Discontinuous Breakwaters", *Int. J. Eng. Model.*, **33**(3-4), 45-61. https://doi.org/10.31534/engmod.2020.3-4.ri.03a.

Barzegar, M. and Palaniappan, D. (2020), "Numerical study on the performance of semicircular and rectangular submerged breakwaters", *Ocean Syst. Eng.*, **10**(2), 201-226. http://dx.doi.org/10.12989/ose.2020.10.2.201.

Beji, S. and Nadaoka, K. (1996), "A formal derivation and numerical modelling of the improved Boussinesq equations for varying depth", *Ocean Eng.*, **23**(8), 691-704. https://doi.org/10.1016/0029-8018(96)84408-8.

Bogucki, D., Haus, B.K. and Shao, M. (2020), February, "*The Response of the Boundary Layer to Weak Forcing*", In Ocean Sciences Meeting 2020. AGU.

Bogucki, D., Haus, B.K. and Shao, M., (2020), February, *The dissipation of energy beneath non-breaking waves*, In Ocean Sciences Meeting 2020. AGU.

Cannata, G., Gallerano, F., Palleschi, F., Petrelli, C. and Barsi, L. (2019), "Three-dimensional numerical simulation of the velocity fields induced by submerged breakwaters", *Int. J. Mech*, **13**, 1-14.

Chasten, M.A., Rosati, J.D., McCormick, J.W. and Randall, R.E. (1993), "*Engineering design guidance for detached breakwaters as shoreline stabilization structures*", US Army Corps of Engineers. http://resolver.tudelft.nl/uuid:8d8157a6-b8a9-43e0-84cf-cfbd1ef1d59e.

Dick, T.M. and Brebner, A. (1969), "Solid and permeable submerged breakwaters", *In Coastal Engineering* 1968, 1141-1158. https://doi.org/10.1061/9780872620131.072.

Dong, G.H., Zheng, Y.N., Li, Y.C., Teng, B., Guan, C.T. and Lin, D.F. (2008), "Experiments on wave transmission coefficients of floating breakwaters", *Ocean Eng.*, **35**(8-9), 931-938. https://doi.org/10.1016/j.oceaneng.2008.01.010.

Esteban, M., Glasbergen, T., Takabatake, T., Hofland, B., Nishizaki, S., Nishida, Y. and Shibayama, T. (2017), "Overtopping of coastal structures by tsunami waves", *Geosciences*, **7**(4), 121. https://doi.org/10.3390/geosciences7040121.

Israeli, M. and Orszag, S.A. (1981), "Approximation of radiation boundary conditions", *J. Comput. Phys.*, **41**(1), 115-135. https://doi.org/10.1016/0021-9991(81)90082-6.

Garcia, N., Lara, J.L. and Losada, I.J. (2004), "2-D numerical analysis of near-field flow at low-crested permeable breakwaters", *Coast. Eng.*, **51**(10), 991-1020. https://doi.org/10.1016/j.coastaleng.2004.07.017.

Ghiasian, M., Rossini, M., Amendolara, J., Haus, B., Nolan, S., Nanni, A., Bel Had Ali, N. and Rhode-Barbarigos, L., (2019), "*Test-Driven Design of an Efficient and Sustainable Seawall Structure*", *Coast. Struct.*, 1222-1227.

Ghiasian, M., Carrick, J., Lirman, D., Baker, A., Ruiz-Merchan, J., Amendolara, J., Haus, B. and Rhode-Barbarigos, L., (2019), "Exploring Coral Reef Restoration for Wave-Energy Dissipation through Experimental Laboratory Testing", *Coast. Struct.*, 975-980.

Ghadimi, P. and Lamouki, M.B.P. (2017), "Finite difference simulation of regular wave propagation over natural beach and composite barriers by Nwogu's extended Boussinesq equations", *Prog. Comput. Fluid Dynam.*, **17**(4), 212-220. https://doi.org/10.1504/PCFD.2017.085178.

Grue, J. and Palm, E. (1985), "Wave radiation and wave diffraction from a submerged body in a uniform current", *J. Fluid Mech.*, **151**, 257-278. https://doi.org/10.1017/S0022112085000957.

Goda, Y. and Suzuki, Y. (1977), "Estimation of incident and reflected waves in random wave experiments", *Coast. Eng*., 828-845. https://doi.org/10.1061/9780872620834.048.

Wei, G. and Kirby, J.T. (1995), "Time-dependent numerical code for extended Boussinesq equations", *J. Waterw. Port, Coast. Ocean Eng.*, **121**(5), 251-261. https://doi.org/10.1061/(ASCE)0733-950X(1995)121:5(251).

Ketabdari, M.J. and Barzegar Paiinlamouki, M. (2014), "Numerical modelling of induced rip currents by discontinuous submerged breakwaters", *Int. J. Marine Sci. Eng.*, **4**(1), 15-24.

Ketabdari, M.J. and Moghaddasi, A. (2015), "Effects of discontinuous submerged breakwater on water surface elevation", *Ocean Syst. Eng.*, **5**(4), 319-329. https://doi.org/10.12989/ose.2015.5.4.319.

Lamberti, A., Archetti, R., Kramer, M., Paphitis, D., Mosso, C. and Di Risio, M. (2005), "European experience of low crested structures for coastal management", *Coast. Eng.*, **52**(10-11), 841-866. https://doi.org/10.1016/j.coastaleng.2005.09.010.

Peregrine, D.H. (1972), "Equations for water waves and the approximations behind them", *Waves on beaches and resulting sediment transport*, 95-121. https://doi.org/10.1016/B978-0-12-493250-0.50007-2.

Madsen, P.A., Murray, R. and Sørensen, O.R. (1991), "A new form of the Boussinesq equations with improved linear dispersion characteristics", *Coast. Eng*., **15**(4), 371-388. https://doi.org/10.1016/0378-3839(91)90017-B.

Matsui, T., SangYeob, L. and Sano, K. (1991), "Hydrodynamic forces on a vertical cylinder in current and waves", *J. Soc. Naval Arch.Japan*, **1991**(170), 277-287. https://doi.org/10.2534/jjasnaoe1968.1991.170_277.

Morison, J.R. (1949), "*Model study of wave action on underwater barriers*", University of California, Berkeley, Fluid Mechanics Laboratory.

Rahman, M.A., Mizutani, N. and Kawasaki, K. (2006), "Numerical modeling of dynamic responses and mooring forces of submerged floating breakwater", *Coast. Eng.*, **53**(10), 799-815. https://doi.org/10.1016/j.coastaleng.2006.04.001.

Raman, H., Shankar, J. and Dattatri, J. (1977), "Submerged breakwaters", *central board of irrigation and power J.* **34**, 205-212.

Rambabu, A.C. and Mani, J.S. (2005), "Numerical prediction of performance of submerged breakwaters", *Ocean Eng*., **32**(10), 1235-1246. https://doi.org/10.1016/j.oceaneng.2004.10.023.

Rojanakamthorn, S., Isobe, M. and Watanabe, A. (1991), "Modeling of wave transformation on submerged breakwater", *Coast. Eng.*, 1060-1073. https://doi.org/10.1061/9780872627765.082.

Seelig, W.N. (1980), "*Two-Dimensional Tests of Wave Transmission and Reflection Characteristics of Laboratory Breakwaters*", Coastal engineering research center Fort belvoi., https://doi.org/10.5962/bhl.title.47373.

Wang, Y., Yin, Z., Liu, Y., Yu, N. and Zou, W. (2019), "Numerical investigation on combined wave damping effect of pneumatic breakwater and submerged breakwater", *Int. J. Naval Archit. Ocean Eng.*, **11**(1), 314-328. https://doi.org/10.1016/j.ijnaoe.2018.06.006.

Wei, G. and Kirby, J.T. (1995), "Time-dependent numerical code for extended Boussinesq equations", *J. Waterw.Port, Coast. Ocean Eng*., **121**(5), 251-261. https://doi.org/10.1061/(ASCE)0733-950X(1995)121:5(251).

Xu, T.J., Wang, X.R., Guo, W.J., Dong, G.H. and Bi, C.W. (2019), "Numerical simulation of the hydrodynamic behavior of a pneumatic breakwater", *Ocean Eng.*, **180**, 108-118. https://doi.org/10.1016/j.oceaneng.2019.04.010.

Zaghian, R., Tavakoli, M. R., Karbasipour, M. and Ahmadabadi, M.N. (2017), " Experimental study of flow structures of a solitary wave propagating over a submerged thin plate in different angles using PIV technique", *Int. J. Heat Fluid Fl*., **66**, 18-26 , https://doi.org/10.1016/j.ijheatfluidflow.2017.05.010.

PL